Pyros: a raster–vector spatial simulation model for predicting wildland surface fire spread and growth

Debora Voltolina[A,B,*] , Giacomo Cappellini[A] , Tiziana Apuani[B] and Simone Sterlacchini[A]

For full list of author affiliations and declarations see end of paper

*Correspondence to:
Debora Voltolina
National Research Council, Institute of Environmental Geology and Geoengineering, Via Mario Bianco 9, 20131 Milan, Italy
Email: debora.voltolina@cnr.it

ABSTRACT

Background. Euro–Mediterranean regions are expected to undergo a climate-induced exacerbation of fire activity in the upcoming decades. Reliable predictions of fire behaviour represent an essential instrument for planning and optimising fire management actions and strategies. **Aims.** The aim of this study was to describe and analyse the performance of an agent-based spatial simulation model for predicting wildland surface fire spread and growth. **Methods.** The model integrates Rothermel's equations to obtain fire spread metrics and uses a hybrid raster–vector implementation to predict patterns of fire growth. The model performance is evaluated in quantitative terms of spatiotemporal agreement between predicted patterns of fire growth and reference patterns, under both ideal and real-world environmental conditions, using case studies in Sardinia, Italy. **Key results.** Predicted patterns of fire growth demonstrate negligible distortions under ideal conditions when compared with circular or elliptical reference patterns. In real-world heterogeneous conditions, a substantial agreement between observed and predicted patterns is achieved, resulting in a similarity coefficient of up to 0.76. **Conclusions.** Outcomes suggest that the model exhibits promising performance with low computational requirements. **Implications.** Assuming that parametric uncertainty is effectively managed and a rigorous validation encompassing additional case studies from Euro–Mediterranean regions is conducted, the model has the potential to provide a valuable contribution to operational fire management applications.

Keywords: agent-based model, Euro–Mediterranean, fire behaviour, fire management, fire suppression, Italy, Rothermel model, Sardinia, spatial simulation model.

Introduction

An annual global average of 400–500 million ha of vegetation burnt between 2002 and 2016 (Giglio *et al.* 2018; Bowman *et al.* 2020). Anthropogenic factors represent the most prevalent source of fire ignitions in Euro–Mediterranean countries (Ganteaume and Syphard 2018; Cattau *et al.* 2020). Moreover, the tendency towards a massive abandonment of traditional rural practices, together with the promptness and effectiveness of fire suppression strategies, is responsible for increasing landscape homogeneity, fuel accumulation and fuel continuity (Turco *et al.* 2016; Kelley *et al.* 2019; Salis *et al.* 2019; Mantero *et al.* 2020). Nevertheless, anthropogenic factors alone are unable to explain the complexity of changes in global fire activity (Pausas and Keeley 2021). Despite uncertainties associated with climate projections, studies at a global and local scale have pointed out the key influence of climate trends in exacerbating fire activity, in terms of either fire season length, fire occurrence or intensity, especially in Euro–Mediterranean regions (Flannigan *et al.* 2009, 2016; Jolly *et al.* 2015; Williams and Abatzoglou 2016; Turco *et al.* 2018; Forkel *et al.* 2019; Dupuy *et al.* 2020).

Accurate simulations of predicted spatiotemporal patterns of fire growth are of prominent importance for planning and optimising prompt intervention strategies to keep the fire spread under control before it could overwhelm the suppression capability of fire management agencies (Tedim *et al.* 2018). The growing availability of computational

resources has fuelled the development of a considerable number of simulators for wildland surface fire behaviour modelling, each characterised by different scales of interest and diverse purpose of the study. Sullivan (2009a, 2009b, 2009c) accomplished an exhaustive review of the strategies adopted to model fire spread and growth, classifying them into three broad categories: (1) physical and quasi-physical models, which take advantage of the fundamental principles of the physics and chemistry of the process of combustion to model the fire spread; (2) empirical and quasi-empirical models, which are essentially based upon statistical analysis of fire spread observations and laboratory or field experiments; and (3) simulation and mathematical analogue models, which implement either of the previous classes of models to simulate the spatial and temporal growth of the flame front in two or three dimensions across a landscape.

Physical and quasi-physical models are renowned for their potential to replicate the emergent behaviour of complex wildland fires. To cite an example, coupled atmosphere–fire models can solve the spatiotemporal variability of airflows over complex terrains while also capturing the fire–atmosphere feedback responsible for fire-induced winds. However, their computational costs still challenge their use in faster-than-real-time applications (Coen 2018). On the other hand, empirical and quasi-empirical models simplify the complexity of the interactions between fire and the environment, resulting in higher computational efficiency. This is one of the rationales behind the widespread use of empirical models as operational tools by fire management agencies (Alexander and Cruz 2013a).

Simulation and mathematical analogue models integrate a broad spectrum of approaches to represent fire growth, ranging from purely vector to purely raster implementations and including a wide variety of hybrid solutions. Popular fire simulators, such as FARSITE (Finney 1998) and Prometheus (Tymstra *et al.* 2010), simulate fire growth by means of a vector implementation based on the Huygens' wavelet principle, which states that each point on the flame front becomes a new source of ignition. Leveraging a Lagrangian approach, such simulators represent the fire front as a closed curve discretised through a growing number of points, each expanding based on a given spread model. As the complexity of the fire front shape increases at each time step, the computational efficiency of the Lagrangian approach is preserved by progressively reducing the number of points approximating the fire front. An increasingly adopted Eulerian alternative to the Lagrangian approach is the level set method (Mallet *et al.* 2009; Ghisu *et al.* 2014; Muñoz-Esparza *et al.* 2018; Alessandri *et al.* 2021). The level set method focuses on the changes that take place at a given point in space as the fire front passes, boasting the advantage of implicitly solving the behaviour of merging fire fronts (Bova *et al.* 2016). At the other end of the spectrum, raster implementations adopt localised sets of evolution rules to simulate fire growth across contiguous neighbouring cells.

The minimum travel time method is a common expansion algorithm used to define the mechanism of interaction between cells and the environment and is frequently expressed by cellular automata (CA) or agent-based models (ABMs). Both CA and ABMs can simulate fire spread and growth as stochastic processes in which the propagation of the fire front towards the neighbouring cells is modelled via a probabilistic approach (Alexandridis *et al.* 2008; Ntinas *et al.* 2017; Freire and Castro DaCamara 2018; Rui *et al.* 2018; Trucchia *et al.* 2020; Katan and Perez 2021), or more rarely, via a deterministic approach using rules based on physical or empirical models (Hernández Encinas *et al.* 2007; Collin *et al.* 2011; Trunfio *et al.* 2011; Ghisu *et al.* 2015; Pais *et al.* 2021). Simplicity of development, better portability to parallel computing environments and higher computational efficiency are among the advantages of raster implementations over vector implementations. Nevertheless, patterns of fire growth predicted by raster implementations can suffer from substantial distortion because of the constraints of the directions of movement that are limited to the number of cells in the neighbourhood; as a result, under homogeneous environmental conditions, the heading portion of the fire front might assume an angular rather than rounded shape (Ghisu *et al.* 2015). The use of larger neighbourhoods partially allows mitigating such distortions under homogeneous conditions, at the cost of an increasing computational effort, and still produces distortions under heterogeneous conditions (Finney 2002). Other approaches were adopted to reduce distortions, such as a hybrid raster–vector implementation, where a local ellipse expands from each cell towards the neighbouring cells without restricting the location of the ignition points to cell centroids (Trunfio *et al.* 2011), or the application of empirical correction factors defined by optimisation processes (Ghisu *et al.* 2015).

The most recent literature reveals the tendency towards the integration of state-of-the-art machine-learning techniques into different fields of wildfire science, including predictive fire behaviour simulation modelling (Jain *et al.* 2020). Some studies trained artificial neural networks to accurately emulate fire growth patterns predicted by different traditional modelling approaches based on vector implementations, e.g. FARSITE or the Lagrangian solver ForeFire (Filippi *et al.* 2010), at a fraction of their computational costs (Hodges and Lattimer 2019; Allaire *et al.* 2021). Fewer studies trained data-driven learning-based algorithms to predict the rate of fire spread based on real-time measurements (Zhai *et al.* 2020) or to predict the areas surrounding a given initial fire perimeter that are expected to burn within the following 24 h (Radke *et al.* 2019). Nevertheless, the limited availability of accurate real-world rate of spread measurements still challenges a wider application of such approaches.

Although existing wildland fire behaviour models serve as valuable foundational tools, there are compelling reasons for considering the development of alternative models rather than relying uniquely on existing ones. Existing models may

not easily adapt to the increasing computational capabilities or the evolving scientific knowledge on fire behaviour without significant modifications. Alternative tailored models can leverage these advancements, potentially providing a more accurate representation of fire dynamics.

This study aims to explore the potential of a hybrid modelling approach to provide reliable and timely information on the expected behaviour of wildland surface fires. The following sections introduce and evaluate the performance of Pyros, a spatial simulation model for predicting patterns of wildland surface fire spread and growth across heterogeneous landscapes. The design and implementation of Pyros spanned 6 years, with the rationale to identify and develop a comprehensive faster-than-real-time modelling framework with potential for operational applications. Pyros strives to complement existing simulators, integrating features from different models. Indeed, Pyros combines the Rothermel quasi-empirical mathematical model (Rothermel 1972), one of the most extensively employed in operational context (Cruz *et al.* 2018), with a hybrid raster–vector implementation of an ABM to simulate fire growth in heterogeneous environmental conditions, potentially capturing and taking advantage of both the physics of fire spread and the dynamic behaviour emerging from ABMs.

Methods

Model overview

Conceptually, Pyros integrates a first subprocess, which computes the metrics relative to the fire spread, and a second subprocess, which simulates the fire growth accordingly.

Fire spread subprocess

Pyros implements a deterministic approach where the magnitude and the prevalent direction of the surface fire spread are defined by the Rothermel quasi-empirical mathematical model (Rothermel 1972), with modifications by Albini (1976). The original formulation of the Rothermel model assumes that a flame propagates with a constant speed in idealised conditions of spatial homogeneity and isotropy, a condition referred to as steady state. However, fire spread is rarely constant in real-world environments, so the steady state assumption requires the explicit definition of a time interval over which fire behaviour properties are constant (Finney *et al.* 2021). Heterogeneity and anisotropy in real-world environments are caused by the spatio-temporal variability in terrain morphology, wind fields and vegetation specific composition, structure, texture and moisture content, which together constitute the input variables to the Rothermel model. The core output of the model is the rate of spread, whose formulation is rooted in the principle of the conservation of energy applied to a unit volume of fuel ahead of an advancing fire in a homogeneous

fuel bed. The rate of spread is expressed by an algebraic relationship between the quantity of heat received by a unit of fuel, namely a heat source, and the quantity of heat required to heat the same unit of fuel to the ignition temperature, referred to as heat sink. The rate of spread R_0 of a fire front propagating on a flat surface through a uniform fuel in the absence of wind is regulated by the relationship:

$$R_0 = \frac{I_r \xi}{\rho_b \varepsilon Q_{ig}}, \ (\text{m min}^{-1}) \tag{1}$$

where the heat source is computed as the product of the reaction intensity I_r times the propagating flux ratio ξ, and the heat sink is defined as the product of the bulk density ρ_b times the effective heating number ε times the heat of preignition Q_{ig}. The maximum upslope rate of spread R_{max} is computed by including the empirical correction factors for slope φ_s and wind φ_w in the computation:

$$R_{max} = R_0 \left(1 + \varphi_s + \varphi_w\right), \ (\text{m min}^{-1}) \tag{2}$$

The maximum rate of spread R_{maxh} relative to the upslope direction is computed as:

$$R_{maxh} = R_0 + \frac{D_h}{t} = R_0$$
$$+ \frac{\sqrt{(D_s + D_w \cos \omega)^2 + (D_w \sin \omega)^2}}{t},$$
$$(\text{m min}^{-1}) \tag{3}$$

where D_h is the vector sum of D_s and D_w, which are functions of the rate of spread R_0 and of the empirical correction factors for slope φ_s and wind φ_w, respectively, ω is the wind direction relative to upslope and t is the elapsed time. Therefore, the direction α of the maximum rate of spread R_{maxh} relative to upslope is:

$$\alpha = \sin^{-1}\left(\frac{|D_w \sin \omega|}{D_h}\right), \ (\text{degrees}) \tag{4}$$

Various adaptations are used in literature to compute the rate of spread in directions other than the upslope. The prevailing approach rests on the assumption that the single mathematical ellipse represents a suitable analytical approximation for patterns of fire growth under idealised homogeneous environmental conditions (Glasa and Halada 2011; Andrews 2018). Despite no physical rationale being available yet and no laboratory or field data on fire growth having rigorously validated this assumption so far, shapes close to perfect ellipses have been observed to emerge from point-source fires in real-world environments (Finney *et al.* 2021). Therefore, for the purpose of this study, the rate of spread is computed in any given direction as a function of the maximum rate of spread R_{maxh} relative to upslope and of the eccentricity of an ellipse with the ignition point located at one of the foci, following Andrews (2018).

Fire growth subprocess

Resting on Rothermel's equations, this study implements a spatially explicit ABM to predict the dynamic behaviour of wildland surface fire and to simulate the expected spatio-temporal patterns of fire growth.

ABMs are a class of flexible computational models that aims to emulate overall system behaviours and to predict complex system-level patterns and properties emerging from the interactions among individual entities, namely agents (Clarke 2014). Agents are discrete autonomous entities processing information and interacting with either the surrounding environment or other agents according to a pre-defined set of rules to make independent decisions and, eventually, learn and adapt to local conditions. The environment is the spatial context in which agents act and interact, and it might be continuous or represented by a grid of discrete raster cells with specific attributes varying in space and time.

The ABM presented in this study includes explicit spatial and temporal dimensions and adopts a hybrid raster–vector approach replicating fire growth by multiple elliptical vector simulations interacting with a discrete raster environment. The modelling approach is inspired by the Huygens' wavelet principle, which considers each point along a fire perimeter as a potential source of new ignition. Starting from any source of ignition, the ABM computes the rate of spread in any direction assuming the fire perimeter to be elliptically shaped and assuming the source of ignition to be in one of the foci of the single mathematical ellipse. To reduce the computational effort, space is discretised into regular hexagonal raster cells with a fixed area and orientation. Time is discretised as well in a regular succession of time steps, namely epochs, which might assume a variable length. The simulation of a succession of discrete epochs allows the model to capture at least part of the intrinsic spatiotemporal variability of time-dependent variables according to the input data availability. Indeed, the model dynamically responds to spatial and temporal variations in the environmental conditions by potentially updating fire spread metrics at every simulation epoch.

The proposed model includes two classes of entities: hexagonal raster cells and fire agents. Fire agents are the sources of ignition of the elliptical fire growth vector simulation, whereas hexagonal raster cells represent the environment fire agents act in and interact with. Each hexagonal raster cell is characterised by state variables that are experienced by the fire agents and can be both static, such as the spatial coordinates of the cell centre, or dynamic, such as the fire spread metrics estimated via the Rothermel's model. The fire spread metrics include the maximum rate of spread relative to upslope, the direction of the maximum rate of spread, the eccentricity of the ellipse approximating the fire growth, and derived metrics such as fire length and width. Dynamic state variables also include an ignition epoch,

defined as the minimum epoch number at which the cell ignites according to the final simulation. A hexagonal mesh was chosen because of its compactness and isotropy: the property of adjacent hexagonal cells with equidistant centres allows the simulation to closely approximate the circular radiation pattern proper of the fire growth under idealised isotropic environmental conditions (de Sousa and Leitão 2018). Each hexagonal raster cell can accommodate one or more fire agents, each representing an individual source of ignition and being characterised by static state variables referring to its spatial coordinates and to the epoch of its activation, i.e. the epoch following that of its emergence.

Model initialisation and procedure

The model initialisation is generic and adaptable to multiple scenarios and geographical sites with different spatial and temporal dimensions. The initialisation begins with the definition of the global conditions experienced by every model entity, including the total number of epochs, their length and the constants describing the geometry of the hexagonal grid cells. The hexagonal raster grid is initialised by using a flat-topped orientation and offsetting odd columns to produce an odd-q vertical layout. Then, for each cell, the model computes the fire spread metrics, namely the magnitude and direction of the maximum rate of spread as well as the fire length and width. For each cell, the ignition epoch is also initialised to a conventional value representing unburnt cells. Finally, the model retrieves a list of the initial ignition points, together with their location and outbreak time, and for each ignition point, instantiates a fire agent within the underlying raster cell. During each model epoch, a scheduler activates all the available fire agents, which take their own actions, eventually updating the ignition epoch of the hexagonal raster cells they interact with.

The model consists of two core classes: the model class, which holds the global attributes, manages the fire agents, and oversees the global level of the model procedure; and the fire agent class. Each instantiation of the model class represents a specific model run including multiple fire agents, which are instantiations of the fire agent class. The implementation of the model procedure can be described iteratively as follows. At the beginning of each epoch, the model: (1) calculates the current epoch t_n; (2) updates the list of fire agents available for that current epoch t_n; and (3) executes the actions of the fire agents by activating them one at a time, following a sequential scheduling. During each epoch t_n, each fire agent: (4) collects updated rate of spread metrics from the hexagonal raster cell; (5) calculates the resulting elliptical growth simulation for the corresponding epoch and the relative rate of spread metrics; (6) computes the location of a variable number of points along the ellipse perimeter; (7) for each point, collects the ignition epoch of the hexagonal raster cell in which the point is

accommodated; and (8) if the ignition epoch is greater than the current epoch t_n, a child fire agent, which will act in the next epoch t_{n+1}, is instantiated in the point location, and the ignition epoch of the hexagonal raster cell is updated setting it to the current epoch t_n. The result of the model procedure iteration over multiple epochs is the simulation of the fire growth pattern that emerges from the ensemble of the ignition epochs of the hexagonal raster cells. Fig. 1 provides a visual representation of the model procedure, whereas Fig. 2 shows a three-epoch simulation run in ideal homogeneous environments.

The spatiotemporal extent of the model is variable and depends on the event scenario. Similarly, the model uses adaptive but proportional spatial and temporal resolution, depending on the event scenario and the available input data. The spatial and temporal resolution of the simulation can be manually adapted to the frequency distribution of the rate of spread values computed by the first model subprocess for the specific extent of the event scenario. For example, given a mean rate of spread of $5 \, \text{m} \, \text{min}^{-1}$ and a coarse spatial resolution, e.g. hexagonal cells with a long diagonal of 125 m in length, an appropriate epoch length would be 25 min. A shorter epoch length, e.g. 5 min, would result in an underestimation of the fire growth because the vector simulation produced during a single epoch would not overstep any of the hexagonal cell boundaries, thus prematurely interrupting the fire growth. Conversely, a larger epoch length, e.g. 50 min, would cause an overestimation of the fire growth because the resulting vector simulation would reach multiple hexagonal cells in a single epoch. In this case, the fire growth might eventually overcome both natural and anthropic obstacles along its path, even if they are observable at the survey scale.

Model testing and validation

Pyros's performance is assessed in qualitative and quantitative terms by comparing the predicted patterns of fire growth with the reference patterns for both ideal and real-world case studies.

Ideal case studies

The model is applied to simulate diverse ideal case studies conceptually grouped into five categories: (1) case no-wind no-slope, including a set of simulation run under simplified environmental conditions assuming the total absence of both the wind and the slope factors; (2) case slope no-wind, where only the slope factor φ_s is introduced to analyse its relative importance on the results; (3) case wind no-slope, where only the wind factor φ_w is introduced and both the vegetation sheltered and unsheltered conditions are tested; (4) case upslope wind, where both the slope factor φ_s and the wind factor φ_w are considered, but only the condition of wind blowing upslope is tested; and (5) case
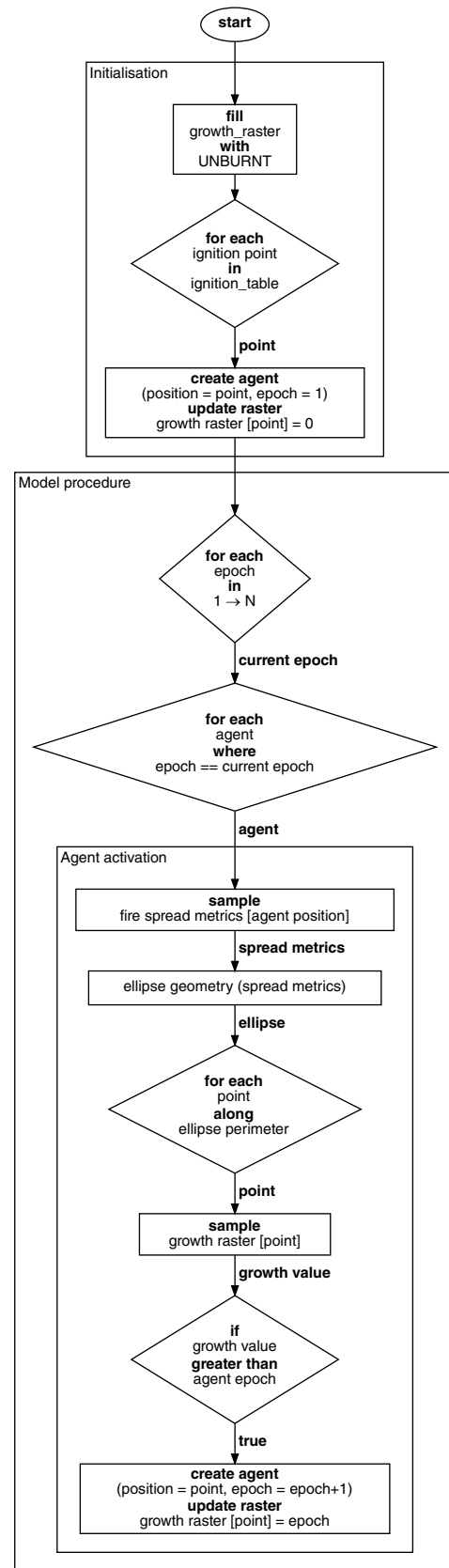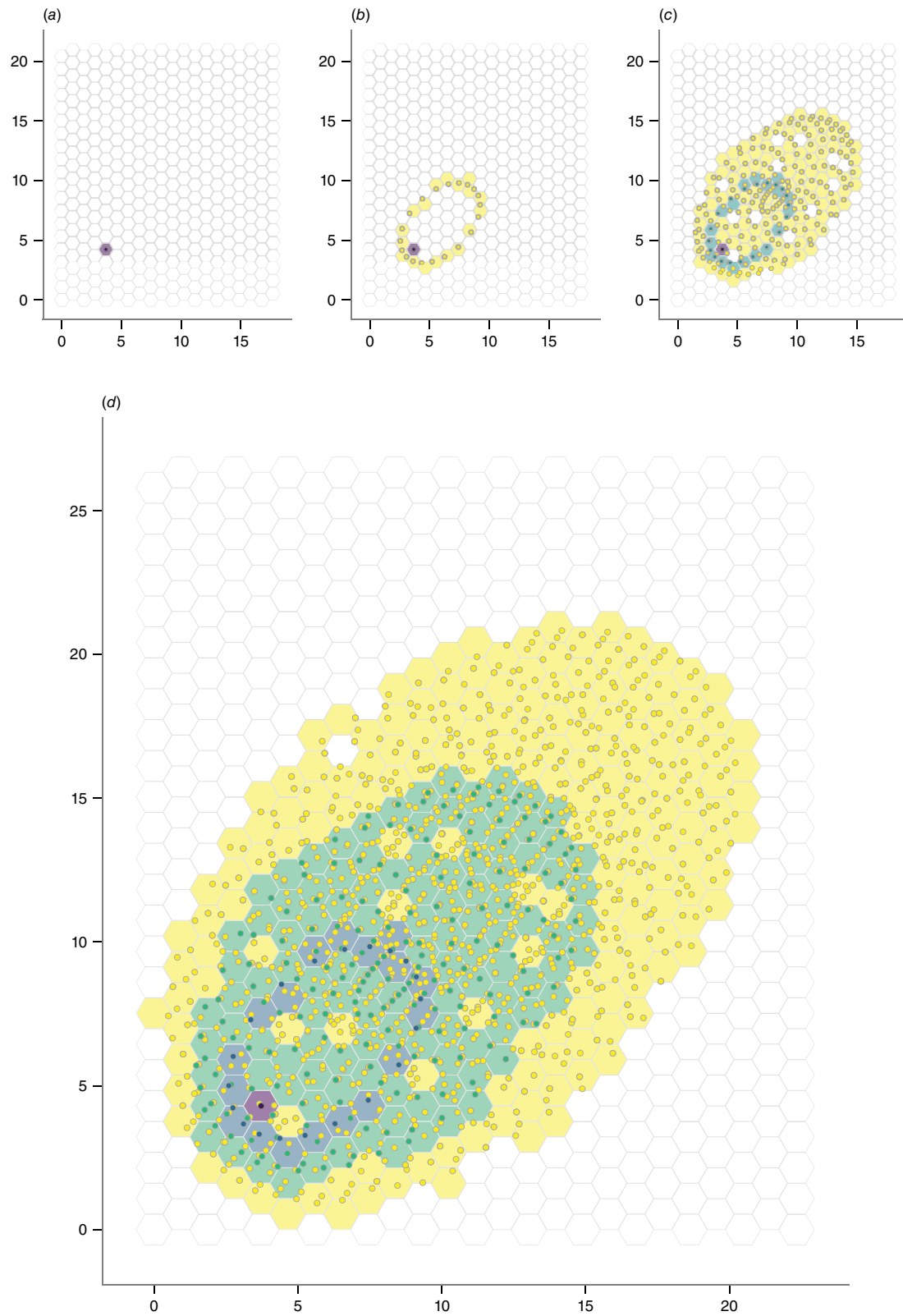

Fig. 1. Flowchart representing the model initialisation and procedure.

Fig. 2. (*Caption on next page*)

Fig. 2. In the initial epoch t_0, a fire agent is instantiated in the location of the initial ignition point to act in the epoch t_1; the ignition epoch of the hosting hexagonal raster cell changes from the unburnt value to 0 (*a*). In the epoch t_1, child fire agents are instantiated along the ellipse perimeter generated by the initial fire agent; the ignition epoch of the hosting hexagonal cells is updated to 1 (*b*). The model procedure is iterated over the epochs t_2 (*c*) and t_3 (*d*). Fire agent colours refer to the epoch of their emergence: purple for the initial epoch, t_0, and yellow for the current epoch. Similarly, cell colours refer to their ignition epoch: white for unburnt.

Table 1. Selected real-world case studies with authoritative information provided by the Autonomous Region of Sardinia, Italy (2017*a*).

	Ignition date	Ignition time (UTC)	Burnt area (ha)	Extinction time (min)
Sagama	24 Aug. 2016	11:20	1841	420
Isili	20 Jul. 2016	09:30	1603	720
Gonnosfanadiga	31 Jul. 2017	12:00	2036	300

cross-slope wind, where both the slope factor φ_s and the wind factor φ_w are considered, and the effects of different wind directions relative to upslope are investigated.

For each category of idealised conditions, different simulations were performed, and the resulting patterns of fire growth were arranged in grids of panels. Each grid compares multiple panels to represent the combined effect of only two changing environmental variables at a time while maintaining the others unchanged. Each panel illustrates a simulation generated under environmental conditions homogeneous in space and time. The spatial and temporal extent and resolution are equal for all the panels in a single grid. The spatial resolution is always 1 m while the temporal resolution varies across grids and ranges from 3 to 6 min, according to the expected rate of spread values. Within each panel, the simulated pattern of fire growth is compared with the reference pattern of fire growth, assuming it to be a single mathematical ellipse built by multiplying the maximum rate of spread value and the eccentricity computed for a single epoch by the total number of simulation epochs.

Real-world case studies

The model is applied to simulate real-world case studies, namely historical fire events that occurred in Sardinia, Italy, between 2016 and 2017. Information available for each event is summarised in Table 1.

Located between 38°51′ and 41°15′N latitude and between 8°8′ and 9°50′E longitude, Sardinia is characterised by complex orographic patterns witnessing the succession of geodynamic events that have occurred in its geological history (Carmignani *et al.* 2016). The climate is typically Mediterranean, with hot and dry summers, marked by prolonged periods of water deficit between May and September, and mild winters with a relatively homogeneous distribution of precipitation over time (Canu *et al.* 2015). The land cover is shaped by anthropic activities and dominated by agricultural lands and pastures, including the typical *dehesas*, agroforestry systems originated by reducing tree density of

Mediterranean forests and shrublands and favouring the grass layer by grazing or crop culture (Moreno and Pulido 2009). Other relevant land cover type includes Mediterranean maquis and garrigue (with *Phyllirea* spp., *Juniperus* spp., *Cistus* spp., *Olea europea* L. var. *sylvestris* Brot., *Arbutus unedo* L., *Erica arborea* L., *Pistacia lentiscus* L., and *Myrtus communis* L.), and broadleaf forests dominated by oak formations with *Quercus ilex* L., *Q. suber* L., and *Q. pubescens* Willd. Needleleaf forests are scarcely represented and primarily include pine plantations with *Pinus pinea* L. and *P. halepensis* Mill. (EEA 2018; Salis *et al.* 2021). According to the Autonomous Region of Sardinia (2020), Sardinia suffers from intense fire seasons, usually lasting from May to October, with the most intense events in July. More than 21 000 wildfire events with an area greater than 0.1 ha occurred in Sardinia between 2005 and 2019, burning an overall surface of 223 543 ha (14 900 ha per year on average).

The selection of real-world case studies was guided by the availability of authoritative information on the location and outbreak time of the ignition points as well as on the delimitation of the fire perimeters. The fire perimeters, namely the observed patterns of fire growth, were detected by the local Forestry Corps of the Autonomous Region of Sardinia through GPS ground surveys and validated through photointerpretation, in compliance with regional and national policies.

Owing to their proximity to wildland–urban interface areas, all the events selected as case studies were subject to intense fire suppression activities including both terrestrial and aerial strategies, mainly dispatched along roads and around residential areas. Information on the timing, location, and effectiveness of fire suppression activities conducted to contain and control the fire growth was retrieved from textual descriptions published in authoritative reports and local chronicles. Despite the high uncertainty related to the lack of georeferenced information, simulations were performed both with and without the implementation of fire suppression interventions because their contribution to

the evolution of the observed fire growth patterns is far from negligible. Fire suppression activities were implemented in the model as barriers consisting of a multiplicative factor of the rate of spread, ranging from zero, for fully successful interventions, to one, for no intervention.

Data collection and preprocessing

Pyros requires both dynamic and static input variables. Dynamic variables, characterised by high temporal variability, such as fuel moisture content and wind speed and direction, are derived through estimations sourced from global reanalysis or remotely sensed assets and products with suitable spatial resolution and revisit periods. Static variables, which exhibit negligible temporal variability over the course of a wildfire, such as terrain morphology or fuel model characteristics, are obtained from institutional datasets.

Information on the spatiotemporal variability of live and dead fuel moisture fractions is derived from optical remote sensing systems by adopting empirical relationships already defined in literature for plant communities in Mediterranean-type climate regions (Chuvieco *et al.* 2004; García *et al.* 2008; Nolan *et al.* 2016), which relate vegetation indices, i.e. the Normalised Difference Vegetation Index (NDVI), with Land Surface Temperature (LST) estimates.

Hourly horizontal wind speed and direction estimates are obtained from the ERA5-Land climatic reanalysis at a spatial resolution of 9000 m (Muñoz-Sabater *et al.* 2021). The mass conserving model implemented by Forthofer *et al.* (2009) is employed to downscale wind data to a 100 m spatial resolution and to model wind field variations induced by local terrain morphology and vegetation patterns. Finally, the wind fields are adjusted to the midflame height that influences the fire spread over surface fuels that are not sheltered by a canopy or through the surface fuel under a forest canopy using the unsheltered or sheltered wind adjustment factors, respectively (Andrews 2012).

Slope and aspect maps are derived from the regional Digital Terrain Model (DTM), available with a 10 m spatial resolution (Autonomous Region of Sardinia 2010).

For each event, a static map of fuel models is generated using an indirect approach. First, the land use map by the Autonomous Region of Sardinia (2008), with a minimum mapping unit of 0.75 ha in rural and natural areas (reference scale 1:25.000), is used as a reference for the definition of homogeneous land cover units. Then, static maps of fuel models are generated by assigning standard (Rothermel 1972; Anderson 1982) and custom fuel models specifically developed for Sardinia (Duce *et al.* 2012) to the land cover units according to Salis *et al.* (2013, 2021).

Static and dynamic input variables are provided to Pyros as independent raster objects with a common reference coordinate system and spatial resolution. The ETRS89 Lambert azimuthal equal-area projection (EPSG:3035) is used to preserve the model applicability at a pan-European scale. The raster objects are resampled to 25 m by using the bicubic method for continuous variables and the mode for discrete variables. Finally, the raster objects are transformed into hexagonal raster objects (de Sousa and Leitão 2017, 2018).

Performance evaluation

Model performance is quantitatively evaluated for ideal and real-world case studies by comparing the predicted patterns of fire growth with the reference ellipse or the actual observed fire growth, respectively. Binary confusion matrices and derived metrics are obtained based on the overlay of the predicted and expected fire growth hexagonal grid maps. The number of correctly classified hexagonal raster cells belonging or not belonging to the burnt class are referred to as true positives, *tp*, and true negatives, *tn*, respectively. Similarly, the number of cells that are either incorrectly assigned to the burnt class or that are not assigned to the burnt class are referred to as false positives, *fp*, or type I errors, and false negatives, *fn*, or type II errors, respectively. Metrics derived from the binary confusion matrix are frequently employed in literature to investigate and evaluate the predictive performance of fire behaviour models (Salis *et al.* 2016; Arca *et al.* 2019; Trucchia *et al.* 2020; Alessandri *et al.* 2021; Katan and Perez 2021; Radočaj *et al.* 2022). In this study, precision and recall were preferred among the derived metrics because they are unaffected by the spatial extent of the simulation domain. The precision is computed as the ratio of *tp* to the total number of cells classified as burnt by the model, namely *tp* plus *fp*. The precision reaches its maximum when the type I error is null. The recall, also referred to as sensitivity or true positive rate, is computed as the ratio of tp to the actual total number of burnt cells, namely *tp* plus *fn*. The recall peaks when the type II error is null.

$$\text{Precision} = \frac{\text{tp}}{\text{tp} + \text{fp}} \qquad (5)$$

$$\text{Recall} = \frac{\text{tp}}{\text{tp} + \text{fn}} \qquad (6)$$

While type II errors are critical for operational fire management purposes, type I errors are more tolerated. However, to obtain a balanced measure that considers both type I and II errors, this study computes the F_1-score, or Sørensen–Dice coefficient, as the harmonic mean of precision and recall. The F_1-score evaluates the similarity between observed and simulated patterns of fire growth as a function of *tp*, *fp*, and *fn*; it varies between zero and one, indicating no agreement or perfect agreement between observed and simulated patterns, respectively.

$$F_1 - \text{score} = \frac{2\text{tp}}{2\text{tp} + \text{fp} + \text{fn}} \qquad (7)$$

Results

Ideal case studies

Pyros was tested under ideal simplified environmental conditions by comparing the predicted patterns of fire growth with the reference circular or elliptical patterns built using the expected rate of spread values predicted by the first model subprocess. Resulting simulations are presented in grids of panels for each category to visually interpret and evaluate the model performance.

Overall, the predicted patterns of fire growth under ideal conditions show a high level of agreement with the reference radial or elliptical patterns. The model exhibits an average F_1-score of 0.97, ranging from 0.80 to 0.99. The average precision is 1.00, indicating a null type I error. The model shows an average recall of 0.95 if excluding cases relative to no-wind no-slope conditions with fuel model 8, where the expected fire spread is too modest to be appreciated at the spatial and temporal scale of the analysis. The high recall indicates minimal, though not entirely negligible, type II errors. Further details regarding these metrics can be found in Supplementary Tables S1–S8.

Case no-wind no-slope

Simulations run under no-wind no-slope ideal conditions resulted in circular radiation patterns, in agreement with the model's theoretical assumptions. The absence of wind and slope allows observing the joint effect of varying live or dead fuel moisture fractions and different fuel models on the predicted patterns of fire growth (Supplementary Figs S1 and S2). As expected, grass fuel models (i.e. models 1, 2, and 3, where grass is the primary fire carrier), and shrub fuel models (i.e. models 4, 5, and 6, where shrubs are the prevalent fire carriers), sustain higher rates of spread compared with forest fuel model (i.e. models 8, 9, and 10, where fire mostly runs through surface fuels, such as forest litter and understorey). Increasing live and dead fuel moisture content reduces the expected spread rates, even though with varying intensity depending on the fuel model. Grass fuel models are more responsive to variations in the dead fuel moisture content, whereas shrub fuel models show a greater sensitivity to variations in the live fuel moisture content. Indeed, the fuel load of grass fuel models is almost exclusively represented by dead material, making these models more susceptible to variations in the dead fuel moisture content. By contrast, the fuel load of shrub fuel models is characterised by a greater fraction of live material, making them more susceptible to variations in the live fuel moisture content.

Case slope no-wind and case wind no-slope

With the introduction of the slope or wind factors, patterns of fire growth assume an elliptical shape: the length-to-width ratio increases with steeper slopes and stronger winds (Supplementary Figs S3 and S4). As expected, similar patterns emerge from the set of simulations run introducing the slope factor alone or the wind factor alone. Again, grass and shrub fuel models sustain higher rates of spread if compared with forest litter or understorey fuel models. This contrast is amplified in the case wind no-slope because of the sheltering effect of the canopy, which is accounted for using the wind adjustment factors (Andrews 2012).

Case upslope, downslope, and cross-slope wind

Finally, the combined influence of wind and slope factors is investigated considering all the possible wind directions relative to upslope, including the two limiting cases of wind blowing upslope and downslope. As expected, the rate of spread is maximum for upslope winds and minimum for downslope winds. Patterns of fire growth produced by jointly increasing slope steepness and varying wind direction indicate that, for a wind speed of 3 m s^{-1} and for slope steepness greater than 20 degrees, the topography seems prevailing in determining the direction of maximum rate of spread (Fig. 3). However, for a wind speed higher than 4 m s^{-1} and a slope steepness of 30 degrees, the wind direction becomes prevalent in determining the direction of the maximum rate of spread (Supplementary Fig. S5). In the limiting case of downslope winds, variations in the predicted patterns produced by the combined effect of increasing slope steepness and increasing wind speed suggest that the slope factor prevails for higher steepness and lower wind speed, whilst the wind factor prevails for lower steepness and higher wind speed (Supplementary Figs S6 and S7).

Real-world case studies

Pyros was validated by simulating three different historical events that occurred in Sardinia, Italy, between July 2016 and July 2017. Pyros was provided with authoritative information on ignition location, outbreak time, and extinction or containment time. Multiple simulations were achieved for each real-world case study to assess the model performance depending on the implementation of fire suppression activities. Barriers were dispatched along roads and around residential and industrial areas as reported by authoritative reports or local chronicles. Resulting simulations with and without fire suppression are reported for each of the three case studies to allow a first qualitative comparison of the predicted patterns. The model exhibits an average F_1-score of 0.56 and 0.65 for simulations performed without or with fire suppression, respectively. The obtained average precision without and with fire suppression is 0.43 and 0.54, respectively, whereas the recall varies between 0.86 and 0.84, respectively. Further details on the metrics can be found in Table 2.

Sagama

The first case study occurred on 24 August 2016, and burnt an overall area of 1841 ha. According to the authoritative
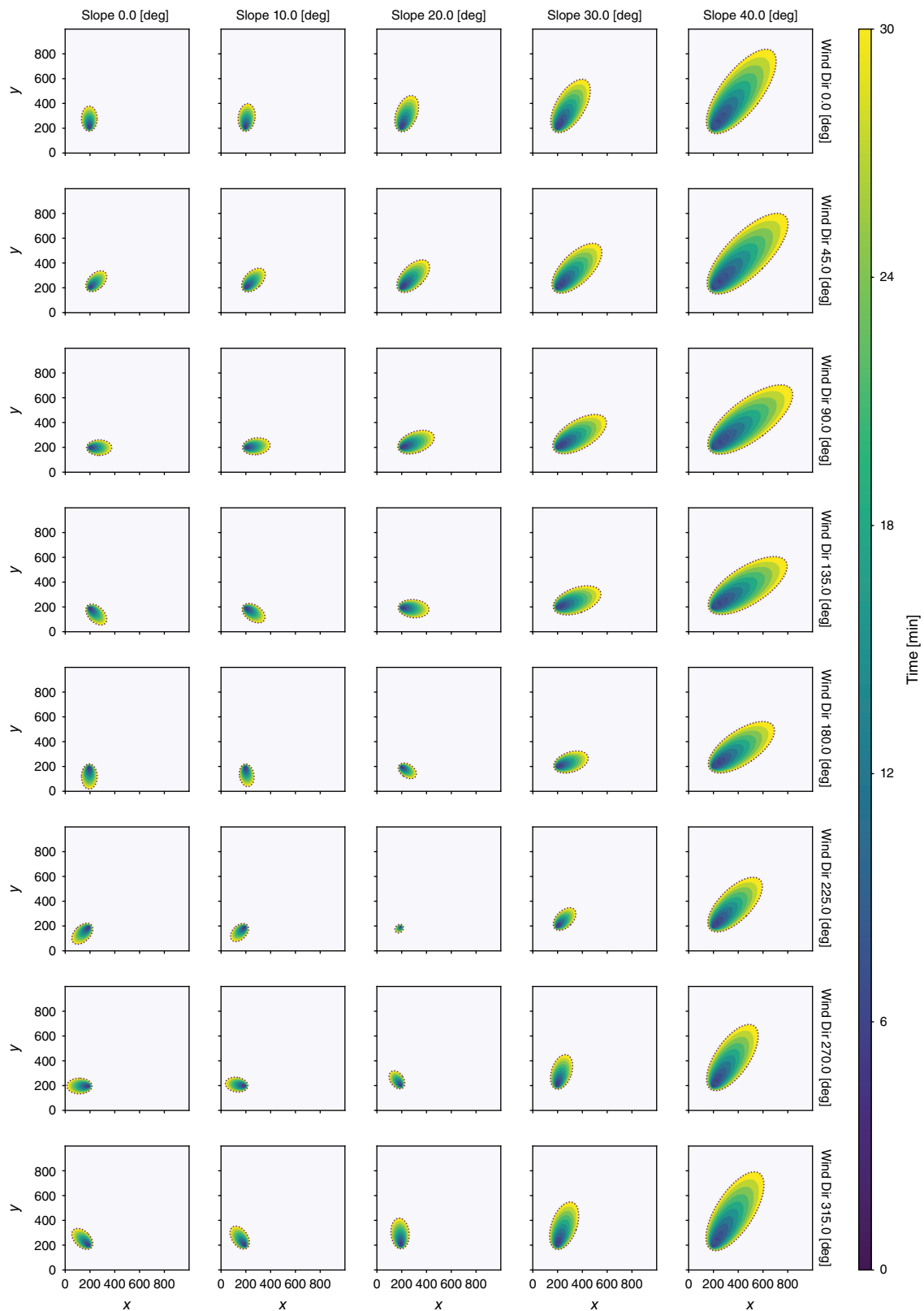
Fig. 3. Case cross-slope wind: slope and wind direction. Input variables: dead fuel moisture fraction is 0.05; live fuel moisture fraction is 1; wind speed at 10 m is 3 m s^{-1}; wind direction varies between 0 and 315 degrees azimuthal; slope varies between 0 and 40 degrees; aspect is 45 degrees azimuthal; fuel model 2 (Rothermel 1972; Anderson 1982). Simulation parameters: 1 m spatial resolution; 10 epochs of 3 min length.

Table 2. Quantitative model performance for the proposed real-world case studies.

Case study	Suppression	Precision	Recall	F_1-score
Sagama	No	0.61	0.89	0.72
	Barriers	0.69	0.86	0.76
Isili	No	0.43	0.81	0.56
	Barriers	0.53	0.80	0.64
Gonnosfanadiga	No	0.26	0.87	0.39
	Barriers	0.41	0.85	0.55

The metrics refer to the comparison between observed and predicted patterns of fire growth for the reported extinction or containment time.

report (Autonomous Region of Sardinia 2017a), the event originated from two distinct ignition points, 2000 m apart from each other, both located in the agricultural land northeast of the urban centre of Sagama, province of Oristano. The flaming front rapidly consumed the cured grasslands, travelling more than 6480 m in less than 420 min. Ground fire suppression activities were dispatched by fire management agencies along both the fire front and the right flank, i.e. the southern and the northwestern regions of the observed pattern of fire growth, respectively, to secure exposed residential areas and anthropogenic assets. Aerial firefighting interventions were dispatched along both fire flanks, but their effects were not simulated in this study because of the high uncertainty in their location, time of occurrence, and effectiveness.

The average head fire rate of spread predicted by the first model subprocess is 14.3 m min^{-1}, 7.1% slower compared with the average head fire rate of spread of 15.4 m min^{-1}, which can be estimated from the observed pattern of fire growth. The comparison between the predicted and the observed pattern of fire growth results in a F_1-score of 0.72 without fire suppression interventions (Fig. 4a). The performance improves with the introduction of barriers dispatched along roads to protect residential areas, resulting in a percentage increase of 5.6% in the F_1-score (Fig. 4b). However, while the implementation of fire suppression activities successfully increases the precision by 11.6%, thus reducing the total overprediction, it also reduces the recall by 3.4%, slightly increasing the total underprediction, reasonably because of an overestimation of the effectiveness of fire suppression actions.

Despite the implementation of fire suppression, fire growth is overpredicted along both fire flanks, i.e. the eastern and western regions of the observed pattern. Conversely, fire growth is systematically underpredicted in the southwestern region. Such discrepancies in the predicted and observed patterns should be ascribed to multiple concomitant reasons. Firstly, the uncertainty in the timing, location, and effectiveness of fire suppression actions led to an intrinsic overprediction of the simulated fire growth pattern along both fire flanks. Secondly, while the authorities reported that the propagation was sustained by northeasterly winds of up

to 8 m s^{-1}, wind speeds reported by the ERA5-Land climate reanalysis are never higher than 4.6 m s^{-1}, thus resulting in an underestimation of the length-to-width ratio of the predicted fire growth. Lastly, results indicate an underestimation of the simulated pattern of fire growth in regions characterised by a higher environmental complexity if compared with the surrounding regions. For example, the southwestern portion of the fire front is unable to overcome a terrain depression placed orthogonally to the direction of the maximum rate of spread, cut through by an intermittent river, and inhabited by a dense riparian broadleaf forest.
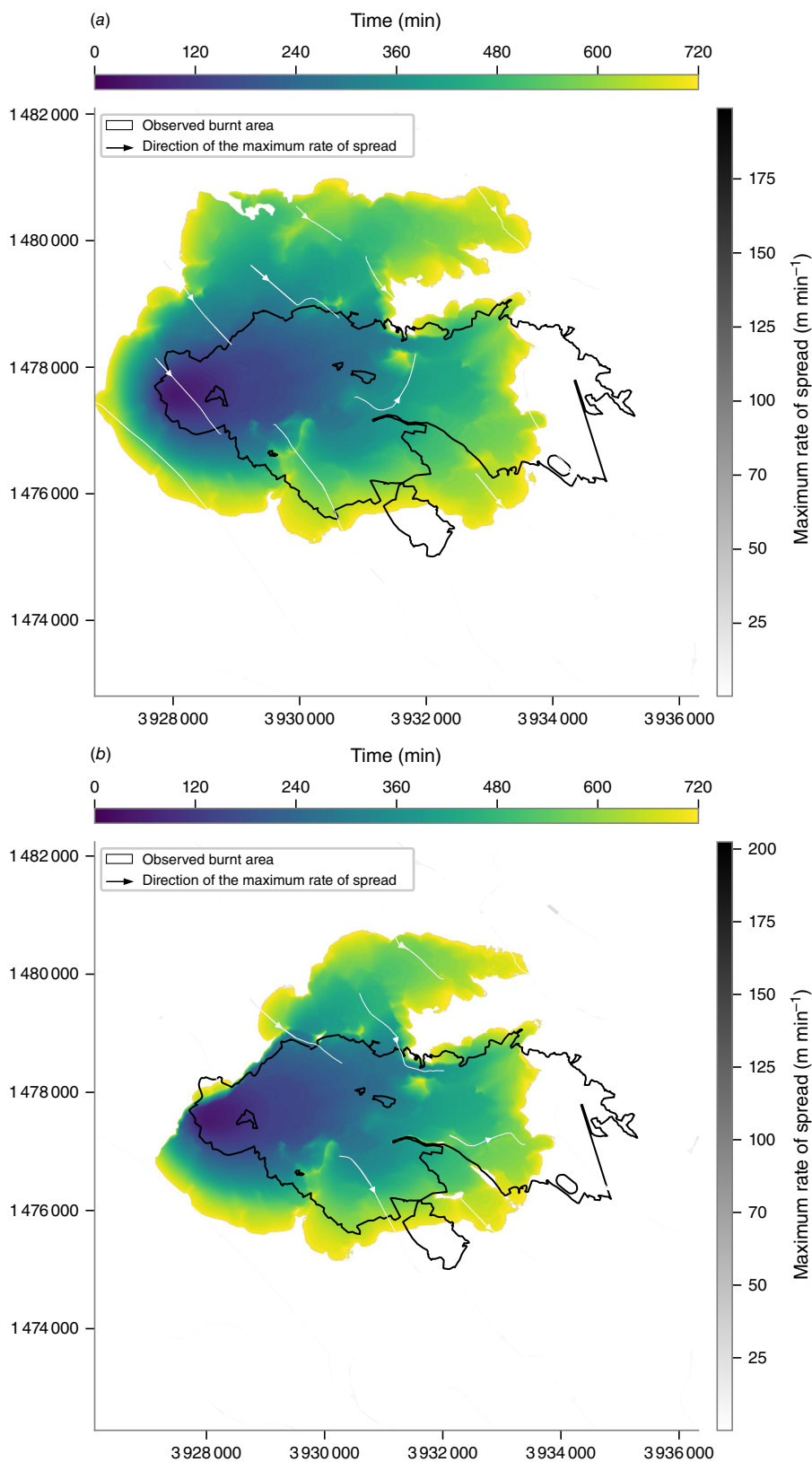
Isili

The second case study occurred on 20 July 2016, and burnt an overall area of 1603 ha. According to the authoritative report (Autonomous Region of Sardinia 2017a), the fire burst out from a single ignition point located in the agricultural land, northwest of the residential area of Isili, province of South Sardinia. Initial ground suppression efforts focused on the left fire flank, i.e. the northwestern region of the observed fire growth. Concurrently, aerial suppression operations targeted the fire front advancing towards northeast through a complex terrain morphology characterised by significant fuel load accumulations. The fire spread was sustained by southwesterly winds reaching velocities of up to 6.9 m s^{-1} and leading to the occurrence of frequent spotting events.

The F_1-score of similarity between predicted and observed patterns without fire suppression interventions is 0.56 (Fig. 5a). The implementation of fire suppression interventions results in a 14.3% increase in the F_1-score (Fig. 5b). The precision increases by 18.9%, from 0.43 to 0.53, partly reducing the overprediction, whereas the recall decreases by 1.2%, from 0.81 to 0.80, slightly increasing the underprediction.

Similarly to the Sagama case study, the simulation of fire suppression interventions alone is not sufficient to explain the overall overprediction, which is particularly evident in the western and northern portions of the predicted pattern of fire growth. It emerges an underestimation of the length-to-width ratio, resulting in an overestimation of both the flanking and backing rates of spread and an underestimation of the heading spread rate. Indeed, the predicted average
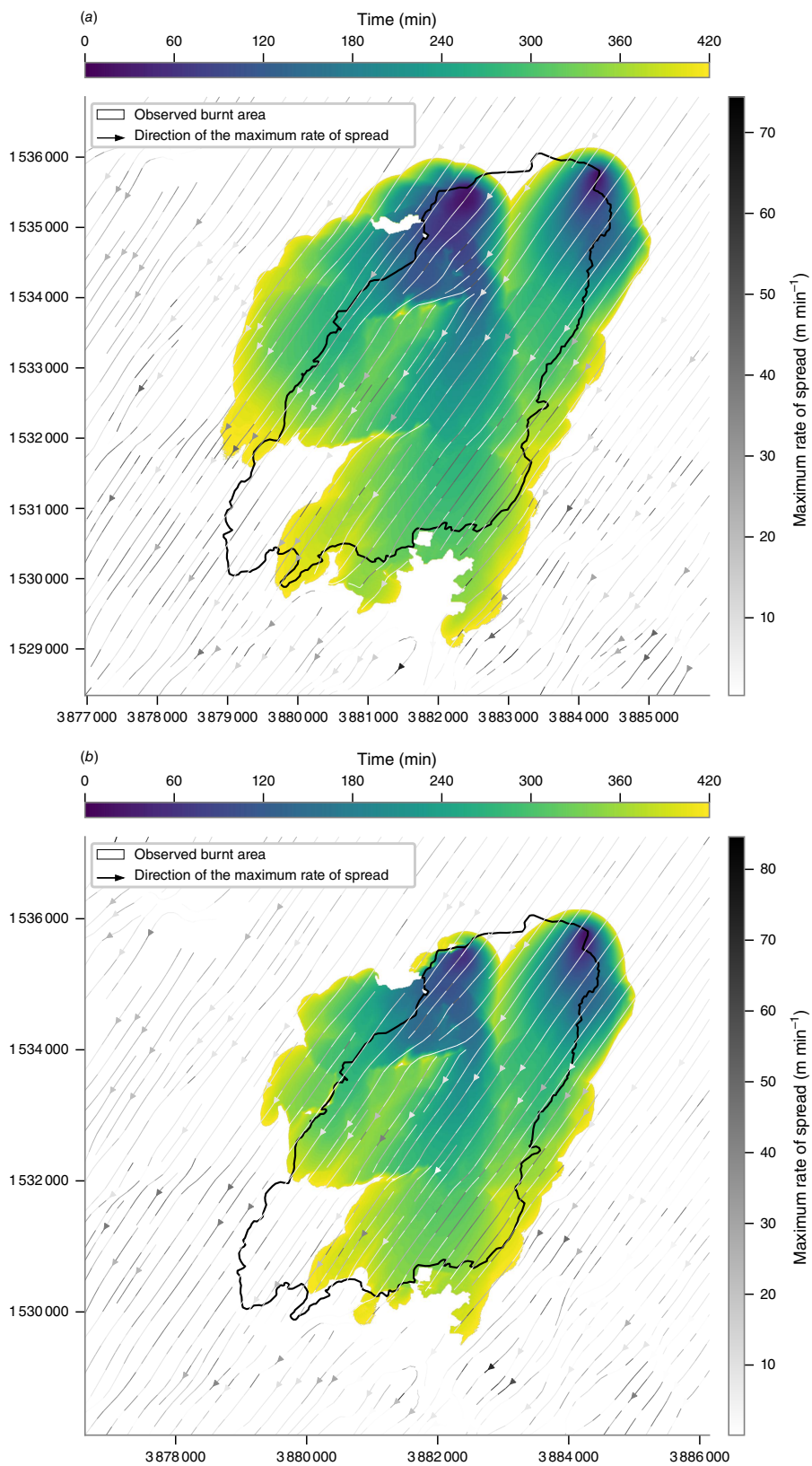
Fig. 4. Sagama case study, 24 August 2016. Predicted patterns of fire growth without (*a*) and with (*b*) the implementation of fire suppression interventions. EPSG:3035.

Fig. 5. Isili case study, 20 July 2016. Predicted patterns of fire growth without (*a*) and with (*b*) the implementation of fire suppression interventions. EPSG:3035.

maximum rate of spread is $8.1 \, \mathrm{m \, min^{-1}}$, 20.6% slower compared with the estimates that can be obtained from the observed pattern, according to which the fire front travelled 7330 m along the west–east direction in 720 min. Also, the hourly wind speed estimated by the ERA5-Land climate reanalysis for the spatial and temporal extent of the event is never higher than $2.2 \, \mathrm{m \, s^{-1}}$, while, according to the authoritative report, wind speed ranged as high as $6.9 \, \mathrm{m \, s^{-1}}$. Furthermore, a west–east gradient of increasing environmental complexity can be observed for this case study, and a complex terrain morphology is known to challenge the mass conserving model by Forthofer *et al.* (2009), which was used to reduce wind fields at the scale of interest (Wagenbrenner *et al.* 2016; Quill *et al.* 2019).

Gonnosfanadiga

The third case study refers to a wildland fire that occurred on 31 July 2017. The local Forestry Corps identified a single ignition point in the agricultural land of Gonnosfanadiga, province of South Sardinia (Autonomous Region of Sardinia 2017b). The event burnt an overall area of 2036 ha, damaging 355 ha of Mediterranean maquis and garrigue of the dune field. Ground fire suppression interventions were dispatched to contain and control the propagation especially along major roads. Aerial fire suppression activities were conducted as well by nine aircraft of the local Forestry Corps and the State air fleet to support ground teams.

The F_1-score of similarity between observed and predicted patterns of fire growth shows a percentage increase of 41.0% following the implementation of ground fire suppression activities along the main roads placed orthogonally to the direction of the maximum rate of spread (Fig. 6a, b). Similarly, the precision increases by 63.4%, from 0.26 to 0.41, while the recall slightly decreases by 2.3%, from 0.87. to 0.85.

Although the simulation of fire suppression interventions resulted in a significant reduction of overall overprediction, the simulated pattern of fire growth still shows overprediction along the heading fire front and the right fire flank, i.e. the western and northwestern portions, respectively. Sustained by southwesterly wind speeds of $7.4 \, \mathrm{m \, s^{-1}}$, the simulated average heading spread rate of $50.0 \, \mathrm{m \, min^{-1}}$ is only 6.4% higher compared with the average heading spread rate of $47.0 \, \mathrm{m \, min^{-1}}$ that is estimated assuming the observed fire front travelled 14 100 m in 300 min. Consequently, the backing fire spread rate is systematically underpredicted, especially in the southeastern region, where vegetation patches classified as dense broadleaf forests also contributed to the observed slowdown of the fire spread and growth.

Discussion

A major issue in fire behaviour modelling is the ability to discern epistemic uncertainty, which is due to the incomplete scientific understanding of fire behaviour, from parametric uncertainty, which stems from the inherent spatial and temporal variability of the environmental conditions (Thompson and Calkin 2011; Finney *et al.* 2013; Cruz *et al.* 2017). From a theoretical perspective, model testing under ideal environmental conditions allows parametric uncertainty to be minimised, thus highlighting the model's strengths and weaknesses. While it is not possible to establish whether a simulation is reliable or not by observing individual metrics or defining thresholds, patterns of fire growth predicted under ideal environmental conditions exhibit a nearly perfect agreement with the expected reference patterns, and show an average similarity quantified as 0.97 in terms of F_1-score. Predicted patterns of fire growth range from circular patterns for fully isotropic conditions to elliptical patterns as the anisotropy increases because of terrain morphology and wind fields. Distortions compared with the target conceptual model are negligible. However, since reference patterns are directly derived from the Rothermel model assuming circular or elliptical patterns of fire growth, model testing with ideal case studies uniquely allows assessment of the performance of the fire growth model subprocess.

Outcomes suggest the model behaves consistently with scientific understanding (although incomplete) of fire behaviour (Finney *et al.* 2021). A remarkable variability in the predicted patterns of fire growth emerges when comparing different fuel models under idealised homogeneous environmental conditions. Grass and shrub fuel models sustain higher rates of spread compared with forest fuel models, where litter and understorey represent the main fire carriers, because of their intrinsically lower fuel loads and the effect of sheltering conditions. The fuel moisture content of live and dead fractions introduces minor variations in the predicted patterns of fire growth compared with wind fields and fuel loads, with marked differences among diverse fuel models depending on their abundance of live or dead fuel loads. Finally, although the infinite variety of wind and slope combinations makes it difficult to generalise the resulting effects on fire behaviour, the combined influence of wind and slope factors on fire spread rates and fire growth patterns is consistent with the available research (Finney *et al.* 2021): the interaction between slope and wind factors exhibits evolutional thresholds compatible with the behaviour of the heading spread rate described in the literature, and both stronger winds and steeper slopes produce similar effects on the resulting patterns of fire growth.

The model performance declines when simulating more complex real-world case studies. Comprehensively, predicted patterns show a level of agreement with observed patterns that is quantified as an average F_1-score of 0.65 for simulations implementing fire suppression activities (Table 2). The heading, backing, and flanking rate of fire spreads are both overpredicted or underpredicted in the diverse case studies. Uncertainty lies in the intrinsic
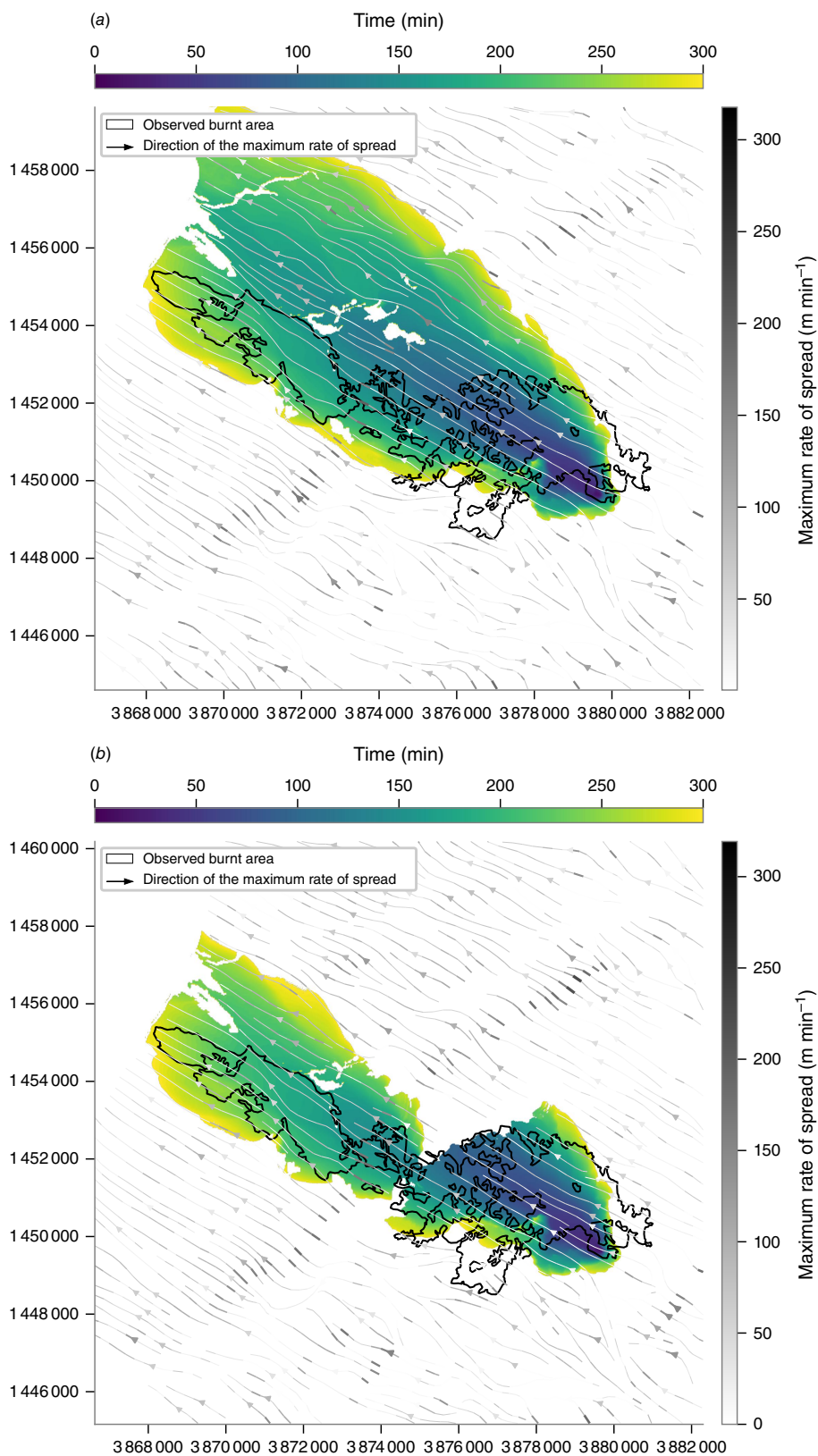
Fig. 6. Gonnosfanadiga case study, 31 July 2017. Predicted patterns of fire growth without (*a*) and with (*b*) the implementation of fire suppression interventions. EPSG:3035.

variability in the environmental conditions, the lack of detailed georeferenced information on the timing, location, and effectiveness of the conducted fire suppression actions, but also in model inaccuracies.

The parametric uncertainty related to the intrinsic variability in space and time of the environmental conditions arguably affected the model performance. Firstly, the model performance decreases with increasing terrain complexity, reflecting both the inheritance of the Rothermel model and the intrinsic uncertainty in wind measurements, with the relative difficulties in downscaling wind fields. Indeed, the mass conserving model employed in this study has already shown reduced accuracy in simulating lee-side flows and in the presence of turbulent rather than laminar flows (Forthofer *et al.* 2014; Wagenbrenner *et al.* 2016). In addition, the model performs better with grass and shrub fuel models, rather than with forest fuel models where the fire is carried by forest litter and understorey, suggesting the need for further investigations into the characterisation of fuel models. The assignment of fuel models to uniform land cover units requires a fully reproducible and less subjective methodology (Finney *et al.* 2021). Furthermore, land cover mapping rarely accounts for the vertical structure and distribution of the understorey, making it difficult to characterise the fuels representing the primary carrier of a surface fire spreading beneath a canopy as well as to estimate the wind speed beneath the canopy. Similarly, the estimation of the fuel moisture fraction in the understorey is challenging, especially when using remotely sensed spaceborne datasets whose estimates are not validated with ground truth derived from either field sampling or continuous monitoring through fuel moisture sticks.

Other major sources of uncertainty are related to the fire suppression activities conducted to control and contain the analysed events. Beside the lack of precise information on the location and timing of intervention, which unquestionably affects the accuracy of the results, suppression effectiveness is also complex to evaluate. The effectiveness of both offensive and defensive tactics is affected by environmental factors, by fire spread rates and intensities, and by specific characteristics of the intervention strategy, including the number of ground and aerial resources deployed, the drop frequency, or the use of suppressant additives on burning fuels rather than retardants applied to unburnt fuels ahead of the fire front (Alexander and Cruz 2013b; Thompson *et al.* 2017; Plucinski 2019a, 2019b). The implementation of fire suppression interventions explains only part of the model overprediction, while in some cases the interventions lead to further underprediction possibly because of an overestimation of their effectiveness. Moreover, the implementation of any fire suppression intervention as a simple barrier oversimplifies the complexity of its impact. Although sufficient to preliminarily assess the model response to fire suppression, this assumption is neither suitable for aerial fire suppression tactics nor ground strategies, such as backfires, where intentional

fires are set along the inner edge of a fuel-free area to consume the fuel ahead of the fire front.

Future perspectives

While outcomes suggest the model is promising, they also indicate there is still room for improvement.

Firstly, a consistent methodology for an accurate and near real-time estimation of the pre-fire environmental conditions needs to be defined and validated. The methodology would benefit from the integration of newly available remote sensing assets and datasets that could provide constantly updated fuel model maps and fuel moisture content estimates to be validated with ground truth. Secondly, improvements in the characterisation of fuel models, especially beneath the canopy, might improve the model's ability to estimate wind speed profiles across the canopy. Finally, while model testing with ideal case studies might represent a preliminary sensitivity analysis, examining the model response to varying one or two factors at a time does not allow a proper exploration of the solution space. Future studies should aim to identify the most relevant sources of parametric uncertainty and estimate the uncertainty propagation through the model to quantify its impact on fire spread and growth.

Additionally, the implementation of a wider range of fire suppression activities through diverse techniques and the use of accurate information on the timing, location, and effectiveness of the interventions would inevitably result in improved model performance.

Furthermore, the model needs to be validated with a wider variety of real-world case studies across Euro–Mediterranean regions to obtain more consistent results on its performance. The proposed selection of real-world case studies strived to capture environmental conditions suitable to illustrate model capabilities and limitations; nevertheless, the selection of case studies is far from being representative of the environmental heterogeneity and complexity observable across Euro–Mediterranean regions. Predicted spatial and temporal patterns of fire growth and their level of agreement with the observed patterns need also to be compared with results obtained by other simulators, such as FARSITE (Finney 1998), FlamMap (Finney and McHugh 2019), or the recently developed ForeFire (Filippi 2018) and Propagator (Trucchia *et al.* 2020) to better contextualise the model in the panorama of the existing simulators.

Computation

Required computations and simulations have been executed on an Intel Core i5-3320M CPU (2 core, 4 threads) 16 GB RAM DD3 1600. Depending on the spatiotemporal extent and resolution of the real-world case study, the estimated total CPU time ranged between 800 and 2000 s. Hence, using all the available logical threads, the computation time varied between 200 and 500 s. The computational

performance of Pyros can be further improved by the implementation of compute kernels to move calculations on accelerators such as graphic processing units (GPU). Preliminary tests using compute shaders on NVIDIA GeForce GTX 1050 resulted in $20\times$ faster computation times on the selected case studies.

Conclusions

Modelling wildland fire behaviour is a remarkably challenging task. The complexity of predicting wildland fire spread and growth lies in handling various sources of uncertainty, ranging from epistemic to parametric uncertainty.

A spatially explicit simulation model for predicting wildland surface fire spread and growth, namely Pyros, was designed and developed. Pyros integrates the Rothermel quasi-empirical equations in a deterministic agent-based model adopting a hybrid raster–vector implementation for predicting patterns of fire growth across heterogeneous environments. The model testing and validation under ideal and real-world conditions allowed a quantitative evaluation of the model performance, highlighting specific strengths and weaknesses. Comprehensively, the model nearly replicated the reference patterns of fire growth under ideal environmental conditions and predicted with a substantial agreement the observed patterns in real-world case studies. The model also exhibited computational performance compatible with faster-than-real-time simulation. Although more robust validation is needed before Pyros can be elevated to the level of an operational tool for supporting fire management strategies and emergency response activities, outcomes are promising, and future research has the potential to improve the model performance by addressing the propagation of parametric uncertainty and minimising causes of both underprediction and overprediction.

Supplementary material

Supplementary material is available online.

References

Albini FA (1976) Computer-based models of wildland fire behavior: a users' manual. General Technical Report. 68 pp. (US Department of Agriculture, Forest Service, Intermountain Forest and Range Experiment Station). Available at https://www.frames.gov/catalog/8178

Alessandri A, Bagnerini P, Gaggero M, Mantelli L (2021) Parameter estimation of fire propagation models using level set methods. *Applied Mathematical Modelling* 92, 731–747. doi:10.1016/j.apm.2020.11.030

Alexander ME, Cruz MG (2013a) Are the applications of wildland fire behaviour models getting ahead of their evaluation again? *Environmental Modelling and Software* 41, 65–71. doi:10.1016/j.envsoft.2012.11.001

Alexander ME, Cruz MG (2013b) Limitations on the accuracy of model predictions of wildland fire behaviour: A state-of-the-knowledge overview. *The Forestry Chronicle* 89, 370–381.

Alexandridis A, Vakalis D, Siettos CI, Bafas G V (2008) A cellular automata model for forest fire spread prediction: The case of the wildfire that swept through Spetses Island in 1990. *Applied Mathematics and Computation* 204, 191–201. doi:10.1016/j.amc.2008.06.046

Allaire F, Mallet V, Filippi J-B (2021) Emulation of wildland fire spread simulation using deep learning. *Neural Networks* 141, 184–198. doi:10.1016/j.neunet.2021.04.006

Anderson HE (1982) Aids to Determining Fuel Models for Estimating Fire Behavior. General Technical Report GTR-122. 22 pp. (US Department of Agriculture, Forest Service, Intermountain Forest and Range Experiment Station). doi:10.2737/INT-GTR-122

Andrews PL (2012) Modeling Wind Adjustment Factor and Midflame Wind Speed for Rothermel's Surface Fire Spread Model. General Technical Report GTR-266. 39 pp. (US Department of Agriculture, Forest Service, Rocky Mountain Research Station) doi:10.2737/RMRS-GTR-266

Andrews PL (2018) The Rothermel Surface Fire Spread Model and Associated Developments: A Comprehensive Explanation. General Technical Report GTR-371. 121 pp. (USUnited States Department of Agriculture, Forest Service, Rocky Mountain Research Station). doi:10.2737/RMRS-GTR-371

Arca B, Ghisu T, Casula M, Salis M, Duce P (2019) A web-based wildfire simulator for operational applications. *International Journal of Wildland Fire* 28, 99–112. doi:10.1071/WF18078

Autonomous Region of Sardinia (2008) Carta dell'Uso del Suolo in scala 1:25.000. Available at http://webgis2.regione.sardegna.it/

Autonomous Region of Sardinia (2010) Digital Terrain Model (10 m). Available at https://www.sardegnageoportale.it/webgis2/sardegnamappe/

Autonomous Region of Sardinia (2017a) Rapporto sugli incendi boschivi e rurali in Sardegna - Anno 2016. (Eds Regione Autonoma della Sardegna - Assessorato alla Difesa dell'Ambiente) [In Italian]. Available at https://www.regione.sardegna.it/documenti/1_274_20170525122956.pdf

Autonomous Region of Sardinia (2017b) Incendio di Arbus - Gonnosfanadiga: un indagato per incendio colposo [In Italian]. Available at https://www.sardegnaambiente.it/index.php?xsl=612&s=344949&v=2&c=4577&idsito=19

Autonomous Region of Sardinia (2020) Sardegna Geoportale - Perimetrazioni aree percorse dal fuoco. Available at http://www.sardegnageoportale.it/webgis2/sardegnamappe/

Bova AS, Mell WE, Hoffman CM (2016) A comparison of level set and marker methods for the simulation of wildland fire front propagation. *International Journal of Wildland Fire* 25, 229–241. doi:10.1071/WF13178

Bowman DMJS, Kolden CA, Abatzoglou JT, Johnston FH, van der Werf GR, Flannigan MD (2020) Vegetation fires in the Anthropocene. *Nature Reviews Earth & Environment* 1, 500–515. doi:10.1038/s43017-020-0085-3

Canu S, Rosati L, Fiori M, Motroni A, Filigheddu R, Farris E (2015) Bioclimate map of Sardinia (Italy). *Journal of Maps* 11, 711–718. doi:10.1080/17445647.2014.988187

Carmignani L, Oggiano G, Funedda A, Conti P, Pasci S (2016) The geological map of Sardinia (Italy) at 1:250,000 scale. *Journal of Maps* 12, 826–835. doi:10.1080/17445647.2015.1084544

Cattau ME, Wessman C, Mahood A, Balch JK (2020) Anthropogenic and lightning-started fires are becoming larger and more frequent over a longer season length in the U.S.A. *Global Ecology and Biogeography* 29, 668–681. doi:10.1111/geb.13058

Chuvieco E, Cocero D, Riaño D, Martin P, Martı'nez-Vega J, de la Riva J, Pérez F (2004) Combining NDVI and surface temperature for the estimation of live fuel moisture content in forest fire danger rating. *Remote Sensing of Environment* 92, 322–331. doi:10.1016/j.rse.2004.01.019

Clarke KC (2014) Cellular Automata and Agent-Based Models. In 'Handbook of Regional Science'. (Eds MM Fischer, P Nijkamp) pp. 1217–1233. doi:10.1007/978-3-642-23430-9

Coen J (2018) Some requirements for simulating wildland fire behavior using insight from coupled weather—wildland fire models. *Fire* 1, 6. doi:10.3390/fire1010006

Collin A, Bernardin D, Séro-Guillaume O (2011) A physical-based cellular automaton model for forest-fire propagation. *Combustion Science and Technology* 183, 347–369. doi:10.1080/00102202.2010.508476

Cruz MG, Alexander ME, Sullivan AL (2017) Mantras of wildland fire behaviour modelling: Facts or fallacies? *International Journal of Wildland Fire* **26**, 973–981. doi:10.1071/WF17097

Cruz MG, Alexander ME, Sullivan AL, Gould JS, Kilinc M (2018) Assessing improvements in models used to operationally predict wildland fire rate of spread. *Environmental Modelling & Software* **105**, 54–63. doi:10.1016/j.envsoft.2018.03.027

de Sousa LM, Leitão JP (2017) Hex-utils: A tool set supporting HexASCII hexagonal rasters. In 'Proceedings of the 3rd International Conference on Geographical Information Systems Theory, Applications and Management (GISTAM)'. pp. 177–183. doi:10.5220/0006275801770183

de Sousa LM, Leitão JP (2018) HexASCII: A file format for cartographical hexagonal rasters. *Transactions in GIS* **22**, 217–232. doi:10.1111/tgis.12304

Duce P, Pellizzaro G, Arca B, Ventura A, Bacciu VM, Salis M, Spano D, Santoni P-A, Barboni T, Leroy V, Cancellieri D, Ferrat L, Perez Y (2012) Fuel types and potential fire behaviour in Sardinia and Corsica islands: a pilot study. In 'Modelling fire behaviour and risk'. (Eds Spano D, Bacciu V, Salis M, Sirca C) pp. 2–8. Available at http://www.cmcc.it/wp-content/uploads/2013/04/P_Book_Modelling-Fire-Behaviour-and-Risk.pdf

Dupuy J-l, Fargeon H, Martin-StPaul N, Pimont F, Ruffault J, Guijarro M, Hernando C, Madrigal J, Fernandes P (2020) Climate change impact on future wildfire danger and activity in southern Europe: a review. *Annals of Forest Science* **77**, 35. doi:10.1007/s13595-020-00933-5

EEA (2018) 'CORINE Land Cover 2018.' (European Union – Copernicus Land Monitoring Service – European Environment Agency)

Filippi JB (2018) ForeFire open source wildfire front propagation model solver and programming interface. *CEUR Workshop Proceedings* **2146**, 87–91.

Filippi JB, Morandini F, Balbi JH, Hill DR (2010) Discrete Event Front-tracking Simulation of a Physical Fire-spread Model. *Simulation* **86**, 629–646. doi:10.1177/0037549709343117

Finney MA (1998) FARSITE: Fire Area Simulator - Model development and evaluation. Research Paper RMRS-RP-4. pp. 1–47. (US Department of Agriculture, Forest Service, Intermountain Forest and Range Experiment Station). doi:10.2737/RMRS-RP-4

Finney MA (2002) Fire growth using minimum travel time methods. *Canadian Journal of Forest Research* **32**, 1420–1424. doi:10.1139/x02-068

Finney MA, McHugh C (2019) FlamMap 6.0. Available at https://www.firelab.org/project/flammap

Finney MA, Cohen JD, McAllister SS, Jolly WM (2013) On the need for a theory of wildland fire spread. *International Journal of Wildland Fire* **22**, 25–36. doi:10.1071/WF11117

Finney M, McAllister S, Grumstrup T, Forthofer J (2021) 'Wildland Fire Behaviour - Dynamics, Principles and Processes.' (CSIRO Publishing: Melbourne) doi:10.1071/9781486309092

Flannigan MD, Krawchuk MA, de Groot WJ, Wotton BM, Gowman LM (2009) Implications of changing climate for global wildland fire. *International Journal of Wildland Fire* **18**, 483–507. doi:10.1071/WF08187

Flannigan MD, Wotton BM, Marshall GA, de Groot WJ, Johnston J, Jurko N, Cantin AS (2016) Fuel moisture sensitivity to temperature and precipitation : climate change implications. *Climatic Change* **134**, 59–71. doi:10.1007/s10584-015-1521-0

Forkel M, Andela N, Harrison SP, Lasslop G, Van Marle M, Chuvieco E, Dorigo W, Forrest M, Hantson S, Heil A, Li F, Melton J, Sitch S, Yue C, Arneth A (2019) Emergent relationships with respect to burned area in global satellite observations and fire-enabled vegetation models. *Biogeosciences* **16**, 57–76. doi:10.5194/bg-16-57-2019

Forthofer JM, Shannon KS, Butler BW (2009) Simulating Diurnally Driven Slope Winds with WindNinja. In 'Proceedings of 8th Symposium on Fire and Forest Meteorological Society'. p. 13. Available at https://www.fs.usda.gov/research/treesearch/61476

Forthofer JM, Butler BW, Wagenbrenner NS (2014) A comparison of three approaches for simulating fine-scale surface winds in support of wildland fire management. Part I. Model formulation and comparison against measurements. *International Journal of Wildland Fire* **23**, 969–981. doi:10.1071/WF12089

Freire JG, Castro DaCamara C (2018) Using cellular automata to simulate wildfire propagation and to assist in fire prevention and fighting. *Natural Hazards and Earth System Sciences Discussions* **19**, 169–179. doi:10.5194/nhess-19-169-2019

Ganteaume A, Syphard A (2018) Ignition Sources. In 'Encyclopedia of Wildfires and Wildland-Urban Interface (WUI) Fires'. (Ed. SL Manzello) pp. 1-17. (Springer International Publishing: Cham.) doi:10.1007/978-3-319-51727-8

García M, Chuvieco E, Nieto H, Aguado I (2008) Combining AVHRR and meteorological data for estimating live fuel moisture content. *Remote Sensing of Environment* **112**, 3618–3627. doi:10.1016/j.rse.2008.05.002

Ghisu T, Arca B, Pellizzaro G, Duce P (2014) A level-set algorithm for simulating wildfire spread. *CMES - Computer Modeling in Engineering and Sciences* **102**, 83–102. doi:10.3970/cmes.2014.102.083

Ghisu T, Arca B, Pellizzaro G, Duce P (2015) An optimal Cellular Automata algorithm for simulating wildfire spread. *Environmental Modelling & Software* **71**, 1–14. doi:10.1016/j.envsoft.2015.05.001

Giglio L, Boschetti L, Roy DP, Humber ML, Justice CO (2018) The Collection 6 MODIS burned area mapping algorithm and product. *Remote Sensing of Environment* **217**, 72–85. doi:10.1016/j.rse.2018.08.005

Glasa J, Halada L (2011) A note on mathematical modelling of elliptical fire propagation. *Computing and Informatics* **30**, 1303–1319.

Hernández Encinas L, Hoya White S, Martín del Rey A, Rodríguez Sánchez G (2007) Modelling forest fire spread using hexagonal cellular automata. *Applied Mathematical Modelling* **31**, 1213–1227. doi:10.1016/j.apm.2006.04.001

Hodges JL, Lattimer BY (2019) Wildland Fire Spread Modeling Using Convolutional Neural Networks. *Fire Technology* **55**, 2115–2142. doi:10.1007/s10694-019-00846-4

Jain P, Coogan SCP, Subramanian SG, Crowley M, Taylor S, Flannigan MD (2020) A review of machine learning applications in wildfire science and management. *Environmental Reviews* **28**, 478–505. doi:10.1139/er-2020-0019

Jolly WM, Cochrane MA, Freeborn PH, Holden ZA, Brown TJ, Williamson GJ, Bowman DMJS (2015) Climate-induced variations in global wildfire danger from 1979 to 2013. *Nature Communications* **6**, 7537. doi:10.1038/ncomms8537

Katan J, Perez L (2021) ABWiSE v1.0: toward an agent-based approach to simulating wildfire spread. *Natural Hazards and Earth System Sciences* **21**, 3141–3160. doi:10.5194/nhess-21-3141-2021

Kelley DI, Bistinas I, Whitley R, Burton C, Marthews TR, Dong N (2019) How contemporary bioclimatic and human controls change global fire regimes. *Nature Climate Change* **9**, 690–696. doi:10.1038/s41558-019-0540-7

Mallet V, Keyes DE, Fendell FE (2009) Modeling wildland fire propagation with level set methods. *Computers & Mathematics with Applications* **57**, 1089–1101. doi:10.1016/j.camwa.2008.10.089

Mantero G, Morresi D, Marzano R, Motta R, Mladenoff DJ, Garbarino M (2020) The influence of land abandonment on forest disturbance regimes: a global review. *Landscape Ecology* **35**, 2723–2744. doi:10.1007/s10980-020-01147-w

Moreno G, Pulido FJ (2009) The Functioning, Management and Persistence of Dehesas. In 'Agroforestry in Europe: Current Status and Future Prospects'. (Eds A Rigueiro-Rodróguez, J McAdam, MR Mosquera-Losada) pp. 127-160. (Springer: Netherlands, Dordrecht) doi:10.1007/978-1-4020-8272-6_7

Muñoz-Esparza D, Kosović B, Jiménez PA, Coen JL (2018) An Accurate Fire-Spread Algorithm in the Weather Research and Forecasting Model Using the Level-Set Method. *Journal of Advances in Modeling Earth Systems* **10**, 908–926. doi:10.1002/2017MS001108

Muñoz-Sabater J, Dutra E, Agustí-Panareda A, Albergel C, Arduini G, Balsamo G, Boussetta S, Choulga M, Harrigan S, Hersbach H, Martens B, Miralles DG, Piles M, Rodríguez-Fernández NJ, Zsoter E, Buontempo C, Thépaut JN (2021) ERA5-Land: A state-of-the-art global reanalysis dataset for land applications. *Earth System Science Data* **13**, 4349–4383. doi:10.5194/essd-13-4349-2021

Nolan RH, Resco de Dios V, Boer MM, Caccamo G, Goulden ML, Bradstock RA (2016) Predicting dead fine fuel moisture at regional scales using vapour pressure deficit from MODIS and gridded weather data. *Remote Sensing of Environment* **174**, 100–108. doi:10.1016/j.rse.2015.12.010

Ntinas VG, Moutafis BE, Trunfio GA, Sirakoulis GC (2017) Parallel fuzzy cellular automata for data-driven simulation of wildfire spreading.

Journal of Computational Science **21**, 469–485. doi:10.1016/j.jocs.2016.08.003

Pais C, Carrasco J, Martell DL, Weintraub A, Woodruff DL (2021) Cell2Fire: A Cell-Based Forest Fire Growth Model to Support Strategic Landscape Management Planning. *Frontiers in Forests and Global Change* **4**, 692706. doi:10.3389/ffgc.2021.692706

Pausas JG, Keeley JE (2021) Wildfires and global change. *Frontiers in Ecology and the Environment* **19**, 387–395. doi:10.1002/fee.2359

Plucinski MP (2019a) Fighting Flames and Forging Firelines: Wildfire Suppression Effectiveness at the Fire Edge. *Current Forestry Reports* **5**, 1–19. doi:10.1007/s40725-019-00084-5

Plucinski MP (2019b) Contain and Control: Wildfire Suppression Effectiveness at Incidents and Across Landscapes. *Current Forestry Reports* **5**, 20–40. doi:10.1007/s40725-019-00085-4

Quill R, Sharples JJ, Wagenbrenner NS, Sidhu LA, Forthofer JM (2019) Modeling Wind Direction Distributions Using a Diagnostic Model in the Context of Probabilistic Fire Spread Prediction. *Frontiers in Mechanical Engineering* **5**, 1–16. doi:10.3389/fmech.2019.00005

Radke D, Hessler A, Ellsworth D (2019) Firecast: Leveraging deep learning to predict wildfire spread. In 'Proceedings of the Twenty-Eighth International Joint Conference on Artificial Intelligence', 10-16 August 2019, Macao, China. (Ed. International Joint Conference on Artificial Intelligence Organization) pp. 4575–4581. doi:10.24963/ijcai.2019/63610.24963/ijcai.2019/636

Radočaj D, Jurišić M, Gašparović M (2022) A wildfire growth prediction and evaluation approach using Landsat and MODIS data. *Journal of Environmental Management* **304**, 114351. doi:10.1016/j.jenvman.2021.114351

Rothermel RC (1972) A Mathematical Model for Predicting Fire Spread in Wildland Fuels. Research Paper INT-115. (US Department of Agriculture, Forest Service, Intermountain Forest and Range Experiment Station) Available at https://www.fs.usda.gov/research/treesearch/32533

Rui X, Hui S, Yu X, Zhang G, Wu B (2018) Forest fire spread simulation algorithm based on cellular automata. *Natural Hazards* **91**, 309–319. doi:10.1007/s11069-017-3127-5

Salis M, Ager AA, Arca B, Finney MA, Bacciu V, Duce P, Spano D (2013) Assessing exposure of human and ecological values to wildfire in Sardinia, Italy. *International Journal of Wildland Fire* **22**, 549–565. doi:10.1071/WF11060

Salis M, Arca B, Alcasena F, Arianoutsou M, Bacciu V, Duce P, Duguy B, Koutsias N, Mallinis G, Mitsopoulos I, Moreno JM, Pérez JR, Urbieta IR, Xystrakis F, Zavala G, Spano D (2016) Predicting wildfire spread and behaviour in Mediterranean landscapes. *International Journal of Wildland Fire* **25**, 1015–1032. doi:10.1071/WF15081

Salis M, Arca B, Alcasena-Urdiroz F, Massaiu A, Bacciu V, Bosseur F, Caramelle P, Dettori S, Fernandes de Oliveira AS, Molina-Terren D, Pellizzaro G, Santoni P-A, Spano D, Vega-Garcia C, Duce P (2019) Analyzing the recent dynamics of wildland fires in Quercus suber L. woodlands in Sardinia (Italy), Corsica (France) and Catalonia (Spain). *European Journal of Forest Research* **138**, 415–431. doi:10.1007/s10342-019-01179-1

Salis M, Arca B, Del Giudice L, Palaiologou P, Alcasena-Urdiroz F, Ager A, Fiori M, Pellizzaro G, Scarpa C, Schirru M, Ventura A, Casula M, Duce P (2021) Application of simulation modeling for wildfire exposure and transmission assessment in Sardinia, Italy. *International Journal of Disaster Risk Reduction* **58**, 102189. doi:10.1016/j.ijdrr.2021.102189

Sullivan AL (2009a) Wildland surface fire spread modelling, 1990-2007. 1: Physical and quasi-physical models. *International Journal of Wildland Fire* **18**, 349–368. doi:10.1071/WF06143

Sullivan AL (2009b) Wildland surface fire spread modelling, 1990-2007. 2: Empirical and quasi-empirical models. *International Journal of Wildland Fire* **18**, 369–386. doi:10.1071/WF06142

Sullivan AL (2009c) Wildland surface fire spread modelling, 1990-2007. 3: Simulation and mathematical analogue models. *International Journal of Wildland Fire* **18**, 387–403. doi:10.1071/WF06144

Tedim F, Leone V, Amraoui M, Bouillon C, Coughlan MR, Delogu GM, Fernandes PM, Ferreira C, McCaffrey S, McGee TK, Parente J, Paton D, Pereira MG, Ribeiro LM, Viegas DX, Xanthopoulos G (2018) Defining Extreme Wildfire Events: Difficulties, Challenges, and Impacts. *Fire* **1**, 9. doi:10.3390/fire1010009

Thompson MP, Calkin DE (2011) Uncertainty and risk in wildland fire management: A review. *Journal of Environmental Management* **92**, 1895–1909. doi:10.1016/j.jenvman.2011.03.015

Thompson MP, Rodríguez y Silva F, Calkin DE, Hand MS (2017) A review of challenges to determining and demonstrating efficiency of large fire management. *International Journal of Wildland Fire* **26**, 562–573. doi:10.1071/WF16137

Trucchia A, D'Andrea M, Baghino F, Fiorucci P, Ferraris L, Negro D, Gollini A, Severino M (2020) Propagator: An operational cellular-automata based wildfire simulator. *Fire* **3**, 26. doi:10.3390/fire3030026

Trunfio GA, D'Ambrosio D, Rongo R, Spataro W, Di Gregorio S (2011) A new algorithm for simulating wildfire spread through cellular automata. *ACM Transactions on Modeling and Computer Simulation* **22**, 1–26. doi:10.1145/2043635.2043641

Turco M, Bedia J, Di Liberto F, Fiorucci P, Von Hardenberg J, Koutsias N, Llasat MC, Xystrakis F, Provenzale A (2016) Decreasing fires in mediterranean Europe. *PLoS One* **11**, e0150663. doi:10.1371/journal.pone.0150663

Turco M, Rosa-Cánovas JJ, Bedia J, Jerez S, Montávez JP, Llasat MC, Provenzale A (2018) Exacerbated fires in Mediterranean Europe due to anthropogenic warming projected with non-stationary climate-fire models. *Nature Communications* **9**, 3821. doi:10.1038/s41467-018-06358-z

Tymstra C, Bryce RW, Wotton BM, Taylor SW, Armitage OB (2010) 'Development and structure of Prometheus: the Canadian Wildland Fire Growth Simulation Model.' (Canadian Forest Service, Northern Forestry Centre: Edmonton, Alberta) Information Report NOR-X-417. 102 p. Available at https://cfs.nrcan.gc.ca/publications?id=31775

Wagenbrenner NS, Forthofer JM, Lamb BK, Shannon KS, Butler BW (2016) Downscaling surface wind predictions from numerical weather prediction models in complex terrain with WindNinja. *Atmospheric Chemistry and Physics* **16**, 5229–5241. doi:10.5194/acp-16-5229-2016

Williams AP, Abatzoglou JT (2016) Recent Advances and Remaining Uncertainties in Resolving Past and Future Climate Effects on Global Fire Activity. *Current Climate Change Reports* **2**, 1–14. doi:10.1007/s40641-016-0031-0

Zhai C, Zhang S, Cao Z, Wang X (2020) Learning-based prediction of wildfire spread with real-time rate of spread measurement. *Combustion and Flame* **215**, 333–341. doi:10.1016/j.combustflame.2020.02.007

Author affiliations

[A]National Research Council, Institute of Environmental Geology and Geoengineering, Via Mario Bianco 9, 20131 Milan, Italy.

[B]Department of Earth Sciences "Ardito Desio", University of Milan, Via Luigi Mangiagalli 34, 20133 Milan, Italy.